

# Automated computer-aided detection of prostate cancer in MR images: from a whole-organ to a zone-based approach

G.J.S. Litjens<sup>a</sup>, J.O. Barentsz<sup>a</sup>, N. Karssemeijer<sup>a</sup> and H.J. Huisman<sup>a</sup>

<sup>a</sup>Radboud University Nijmegen Medical Centre, Nijmegen, The Netherlands;

## ABSTRACT

MRI has shown to have great potential in prostate cancer localization and grading, but interpreting those exams requires expertise that is not widely available. Therefore, CAD applications are being developed to aid radiologists in detecting prostate cancer. Existing CAD applications focus on the prostate as a whole. However, in clinical practice transition zone cancer and peripheral zone cancer are considered to have different appearances. In this paper we present zone-specific CAD, in addition to an atlas based segmentation technique which includes zonal segmentation. Our CAD system consists of a detection and a classification stage. Prior to the detection stage the prostate is segmented into two zones. After segmentation features are extracted. Subsequently a likelihood map is generated on which local maxima detection is performed. For each local maximum a region is segmented. In the classification stage additional shape features are calculated, after which the regions are classified. Validation was performed on 288 data sets with MR-guided biopsy results as ground truth. Free-response Receiver Operating Characteristic (FROC) analysis was used for statistical evaluation. The difference between whole-prostate and zone-specific CAD was assessed using the difference between the FROCs. Our results show that evaluating the two zones separately results in an increase in performance compared to whole-prostate CAD. The FROC curves at .1, 1 and 3 false positives have a sensitivity of 0.0, 0.55 and 0.72 for whole-prostate and 0.08, 0.57 and 0.80 for zone-specific CAD. The FROC curve of the zone-specific CAD also showed significantly better performance overall ( $p < 0.05$ ).

**Keywords:** Computer aided detection, prostate cancer, MRI, zone-specific

## 1. INTRODUCTION

Prostate cancer is the most prevalent noncutaneous cancer in men.<sup>1</sup> MRI has shown to have great potential in the localization and grading of this disease.<sup>2,3</sup> However, reading prostate MRI requires substantial experience<sup>4</sup> and is time-consuming. Computer-aided detection (CAD) applications have been developed to aid radiologists in detecting and diagnosing cancer.<sup>5-7</sup> Most current CAD applications focus on the prostate as a whole, however, the prostate consists of three zones of which two are clearly visible in MRI, the transition and peripheral zone. In clinical practice transition zone and peripheral zone cancers are considered to have distinctly different appearances,<sup>8,9</sup> however this is not yet considered in current computer-aided detection systems. In this paper we investigate the use of zone-specific CAD to detect prostate cancer compared to whole-prostate CAD. An important aspect of zone-specific CAD is the segmentation of the prostate zones. An atlas-based method to segment the prostate zones is also presented. Furthermore, we perform a feature selection experiment to investigate if the zones are characterized by different features.

## 2. METHODS

### 2.1 Segmentation of prostate zones

The prostate zone segmentation is an atlas-based method, which follows a similar approach to the one presented by Klein et al.<sup>13</sup> The T2-weighted sequences of the atlases, which best represent anatomical details, are registered to the new cases. The metric used is normalized mutual information. In our system we use 50 atlases in which the peripheral zone and the prostate were segmented. The selection of these atlases is based on the following criterion:

$$r_i = \frac{\text{NMI}(P, A_i \circ T_i)}{\max_j \text{NMI}(P, A_j \circ T_j)} \quad (1)$$

Table 1. Overview of voxel features used in the CAD system.

Name	Type	Description
ADC	Intensity	Apparent diffusion coefficient, measure for cellular density
$K_{\text{trans}}$	Intensity	Pharmacokinetic parameter, related to vessel permeability
$k^{\text{ep}}$	Intensity	Pharmacokinetic parameter, related to permeability and extracellular volume
Late Wash	Intensity	Pharmacokinetic parameter, related to the washout of contrast agent
T2W	Intensity	T2-weighted voxel grey value, related to voxel T2
Homogeneity	Texture	Co-occurrence matrix <sup>10</sup> based texture feature, related to the homogeneity of the region around the voxel
Texture Strength	Texture	Neighborhood Gray-Tone Difference Matrix <sup>11</sup> based texture feature, related to strength of texture around a voxel
ADC Blob	Blob detection	Multi-scale Hessian blob detection <sup>12</sup> on ADC map
$K_{\text{trans}}$ Blob	Blob detection	Multi-scale Hessian blob detection on $K_{\text{trans}}$ map
$k^{\text{ep}}$ Blob	Blob detection	Multi-scale Hessian blob detection on $k^{\text{ep}}$ map
Late Wash Blob	Blob detection	Multi-scale Hessian blob detection on Late Wash map

Here P and A are the patient and atlas image, and T the transform resulting from the registration. NMI is the normalized mutual information and  $r$  is used as a selection criterion, which has a value between 0 and 1. When the selection criterion equals 1, one atlas is selected, when equals 0 all atlases are selected. In our experiments  $r$  was set to 0.8. Atlases are selected for the prostate and for the peripheral zone separately. Equation 1 is only evaluated within the transformed manual segmentation of the registered atlas. The transition zone segmentation is constructed by taking the difference of the prostate and peripheral zone segmentations. An example is shown in figure 1.

## 2.2 CAD system

The CAD system can be presented as a flowchart (figure 2). Firstly, the prostate is segmented into the two different zones, the peripheral and transition zone, as discussed in the previous subsection.

Secondly, voxel features are extracted for each zone. These features are extracted from the MR images, which consist of an apparent diffusion coefficient (ADC) map, a dynamic contrast enhanced (DCE) time series and T2-weighted images. In addition, pharmacokinetic parameter maps were calculated from the DCE series.<sup>14, 15</sup> A full list of all features is presented in table 1.

Thirdly, the feature vector for each voxel is classified by a k-Nearest Neighbor (kNN) classifier ( $k = \sqrt{N}$ ). This results in a likelihood map per zone, which represent the likelihood that a voxel is part of a malignant

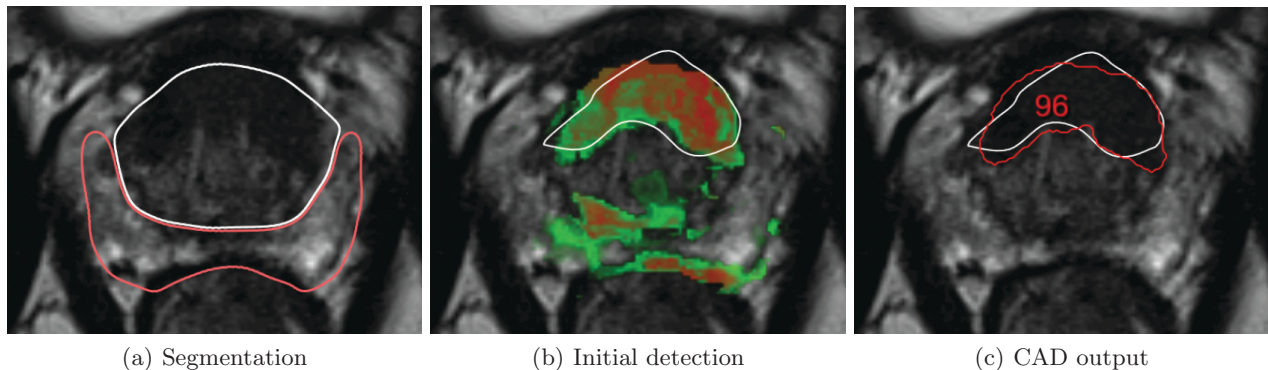


Figure 1. The zone-specific CAD pipeline in images: in the left image the segmentation results are shown with the peripheral zone in pink and the transition zone in white. In the middle image the ground truth is shown as a white contour on top of the voxel likelihood map, where red corresponds to high likelihood of malignancy ( $> 0.8$ ), green areas to a likelihood between 0.2 and 0.8 and transparent areas to 0 to 0.2. The right image shows the final output of the CAD system with the lesion segmentation and region likelihood overlaid on the ground truth.

Table 2. Overview of the region features used in the CAD system. Here 25p and 75p mean the 25th and the 75th histogram percentile of the feature within the segmented region.

Name	Type	Description
ADC <sub>25p</sub>	Intensity	Apparent diffusion coefficient, measure for cellular density
$K_{trans,75p}$	Intensity	Pharmacokinetic parameter, related to vessel permeability
$k^{ep,75p}$	Intensity	Pharmacokinetic parameter, related to permeability and extracellular volume
Late Wash <sub>25p</sub>	Intensity	Pharmacokinetic parameter, related to the washout of contrast agent
T2W <sub>25p</sub>	Intensity	T2-weighted voxel grey value, related to voxel T2
Homogeneity <sub>75p</sub>	Texture	Co-occurrence matrix <sup>10</sup> based texture feature, related to the homogeneity of the region around the voxel
Texture Strength <sub>75p</sub>	Texture	Neighborhood Gray-Tone Difference Matrix <sup>11</sup> based texture feature, related to strength of texture around a voxel
ADC Blob <sub>75p</sub>	Blob detection	Multi-scale Hessian blob detection <sup>12</sup> on ADC map
$K_{trans}$ Blob <sub>75p</sub>	Blob detection	Multi-scale Hessian blob detection on $K_{trans}$ map
$k^{ep}$ Blob <sub>75p</sub>	Blob detection	Multi-scale Hessian blob detection on $k^{ep}$ map
Late Wash Blob <sub>75p</sub>	Blob detection	Multi-scale Hessian blob detection on Late Wash map
Likelihood <sub>75p</sub>	Intensity	75th percentile of the voxel likelihood within the segmented region.
Volume	Shape	The volume of the lesion.
Compactness	Shape	Compactness of the lesion, measure for irregularity of lesion shape.
Sphericity	Shape	Measure for how similar the lesion is to a sphere.

lesion.

Fourthly, local maxima detection is performed on the likelihood maps using a spherical window with a diameter of 10 mm. After initial local maxima detection the local maxima which are less than 10 mm apart are merged. This merging step replaces the initial local maxima with a new local maximum using the mean position of the initial local maxima. These positions are weighted according to their likelihood value. The original likelihood of the of the local maximum with the highest likelihood is propagated to this new local maximum. This is iterated until no more merging occurs.

Fifthly, the local maxima are used to segment a candidate using a region growing and morphology based method which has been previously applied to breast MR and lung nodule segmentation in CT,<sup>16</sup> afterwards the region features are calculated (Table 2).

Finally, the region feature vectors are classified using a SVM classifier for each zone. The SVM uses a radial basis kernel and the parameters  $C$  and  $\gamma$  are optimized using a grid search. This results in a likelihood per region.

### 3. VALIDATION

#### 3.1 Patient data

In total 288 patients who underwent MR-guided biopsy were included in our validation, of which 121 had prostate cancer. The other 167 patients had negative biopsies. Segmentation of cancer regions was performed by

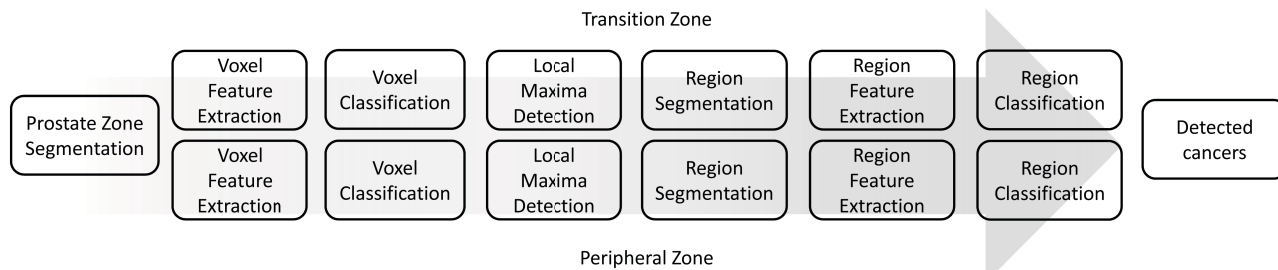


Figure 2. Flowchart of the CAD system

Table 3. Selected features for the peripheral and transition zones for both voxel and region classification stages. The order of the features corresponds to the amount of times they were selected in the cross-validation. Area under the ROC curve (Az) of the leave-one-patient-out cross-validation after each selection step is located to the right of the selected feature

Voxel	Feature 1	Az	Feature 2	Az	Feature 3	Az	Feature 4	Az	Feature 5	Az
PZ	ADC	0.755	$k^{ep}$ Blob	0.815	$k^{ep}$	0.823	Late Wash Blob	0.826	Late Wash	0.828
TZ	ADC	0.822	ADC Blob	0.846	$k^{ep}$	0.847	Texture Strength	0.848	$K_{trans}$	0.848
Region	Feature 1	Az	Feature 2	Az	Feature 3	Az	Feature 4	Az	Feature 5	Az
PZ	$K_{trans,75p}$	0.762	$K_{trans}$ Blob <sub>75p</sub>	0.785	Volume	0.791	Sphericity	0.797	Compactness	0.802
TZ	Likelihood <sub>75p</sub>	0.754	ADC <sub>75p</sub>	0.798	Compactness	0.821	Sphericity	0.840	Volume	0.853

an image analyst based on point annotations of an experienced radiologist (20 years of experience with prostate MR). Cancers were assigned to a zone by a radiologist. In total we found 88 transition zone cancers and 55 peripheral zone cancers for a total of 133 malignant lesions.

### 3.2 CAD evaluation

For CAD evaluation a leave-one-patient-out cross-validation approach was chosen. The voxel feature training data was extracted from the segmented cancers regions. Healthy voxels were randomly sampled within each zone which resulted in balanced training data. Region feature training data was extracted from the manual segmentations of cancer regions and false positive regions after first stage classification. CAD performance was evaluated using FROC curves. A CAD mark was considered a true positive when the automated region segmentation overlapped the center of the manually segmented region, all others were considered false positives (FPs). FPs were only considered in healthy patients. The FROC curves of the whole-prostate and zone-specific CAD systems were statistically compared using JAFROC.<sup>17</sup> The figure of merit used was the area under the alternative FROC (AFROC) curve. For the whole-prostate system the whole prostate is considered as one zone, the rest of the system is equal to the zone-specific system.

### 3.3 Feature Selection

To further investigate the differences between the zones a feature selection experiment was performed. The final voxel and region training data was subjected to a sequential forward floating feature selection<sup>18</sup> using a kNN

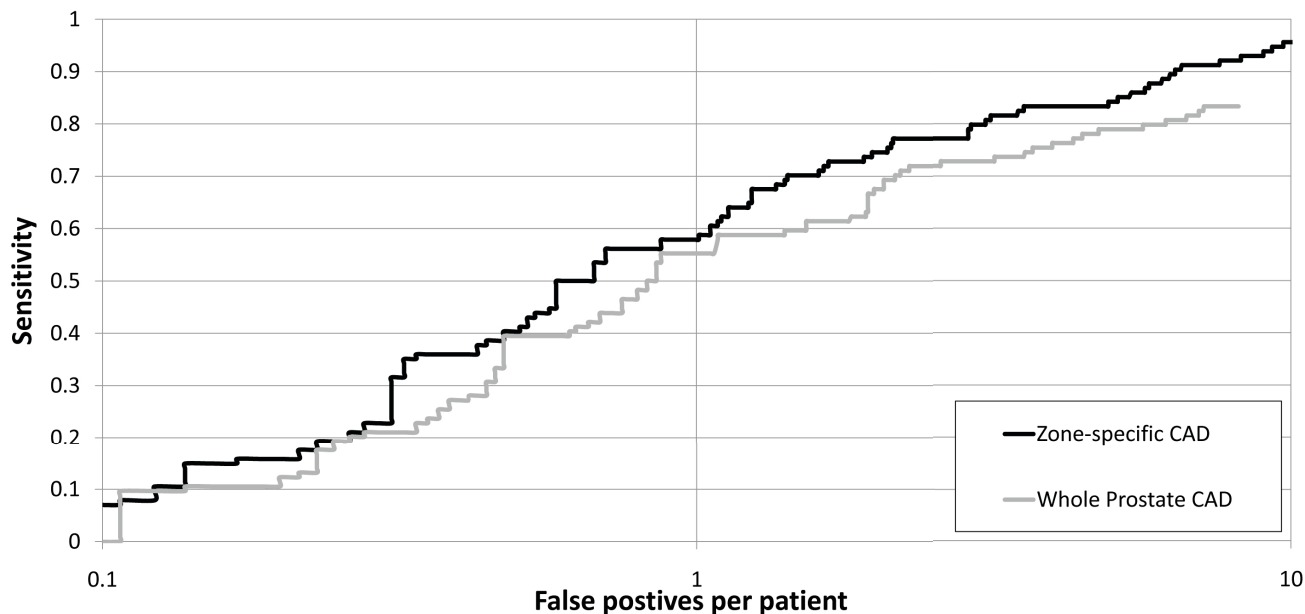


Figure 3. Classification results presented in an FROC curve.

classifier ( $k = \sqrt{N}$ ). Selection was performed on the basis of the area under the receiver-operating characteristic curve and in a leave-one-patient-out cross-validation. The five features that were chosen were selected most often, sorted on the amount of times they were selected.

## 4. RESULTS

### 4.1 CAD evaluation

The results of the CAD evaluation are presented in figure 3. The FROC curve for zone-specific CAD is at a higher sensitivity for almost the entire range of FPs per patient. Specifically, at 0.1, 1 and 3 FPs per patient the sensitivity is 0.08, 0.57 and 0.80 for zone-specific and 0.0, 0.55 and 0.72 for whole-prostate CAD. The analysis using JAFROC<sup>17</sup> shows that the difference between the FROC curves is significant ( $p < 0.05$ ).

### 4.2 Feature Selection

Feature selection results are summarized in table 3. The table shows that different features are selected for the peripheral and transition zone. For the voxel features we see that the ADC value is very important for both zones. The peripheral zone classifier focusses more on the features that are related to pharmacokinetics, i.e. wash-out, whereas the transition zone classifier focusses more on texture and initial enhancement pharmacokinetics, i.e.  $K_{trans}$ . In the region classification both zonal classifiers select all the shape based features. However, the most important features are quite different. The peripheral zone classifier now focusses on  $K_{trans}$  whereas the transition zone classifier uses the voxel likelihood as the most important feature.

## 5. DISCUSSION

In this paper we have shown that using zone-specific CAD for prostate cancer detection can increase performance over whole-prostate CAD. FROC curves show improvement at almost all false positive levels. Feature selection further validates the use of a zone-specific system, as different features are selected for the zones at voxel and region classification stages. Atlas-based segmentation of the zones is accurate enough to show an increase in CAD performance compared to the whole-prostate system. Although this study shows the feasibility of a zone-specific CAD system, there are some limitations. Improving the segmentation will reduce the false positives that occur due to candidates being classified in the wrong zone. The segmentation also requires substantial computing power, we use a cluster to keep segmentation time under 10 minutes, improvement of the segmentation method should also focus on decreasing computation time. In addition, one of the powerful opportunities the binary segmentation of the different zones provides, namely the ability to use different and more specific features for each zone has not yet been investigated. Summarizing, zone-specific prostate cancer detection has shown to outperform classical whole-prostate cancer detection. In addition we presented a segmentation technique for the individual prostate zones that is accurate enough for use in CAD systems.

## REFERENCES

- [1] Jemal, A., Siegel, R., Xu, J., and Ward, E., "Cancer statistics, 2010," *CA Cancer J Clin* **60**, 277–300 (2010).
- [2] Tanimoto, A., Nakashima, J., Kohno, H., Shinmoto, H., and Kuribayashi, S., "Prostate cancer screening: the clinical value of diffusion-weighted imaging and dynamic MR imaging in combination with T2-weighted imaging," *J Magn Reson Imaging* **25**(1), 146–152 (2007).
- [3] Kitajima, K., Kaji, Y., Fukabori, Y., Yoshida, K., Suganuma, N., and Sugimura, K., "Prostate cancer detection with 3 T MRI: comparison of diffusion-weighted imaging and dynamic contrast-enhanced MRI in combination with T2-weighted imaging," *J Magn Reson Imaging* **31**(3), 625–631 (2010).
- [4] Lim, H. K., Kim, J. K., Kim, K. A., and Cho, K.-S., "Prostate cancer: apparent diffusion coefficient map with T2-weighted images for detection—a multireader study.," *Radiology* **250**(1), 145–151 (2009).
- [5] Langer, D. L., van der Kwast, T. H., Evans, A. J., Trachtenberg, J., Wilson, B. C., and Haider, M. A., "Prostate cancer detection with multi-parametric MRI: logistic regression analysis of quantitative T2, diffusion-weighted imaging, and dynamic contrast-enhanced MRI.," *J Magn Reson Imaging* **30**(2), 327–334 (2009).

- [6] Artan, Y., Haider, M. A., Langer, D. L., van der Kwast, T. H., Evans, A. J., Yang, Y., Wernick, M. N., Trachtenberg, J., and Yetik, I. S., "Prostate cancer localization with multispectral mri using cost-sensitive support vector machines and conditional random fields.," *IEEE Trans Image Process* **19**(9), 2444–2455 (2010).
- [7] Vos, P. C., Hambrock, T., Barentsz, J. O., and Huisman, H. J., "Computer-assisted analysis of peripheral zone prostate lesions using t2-weighted and dynamic contrast enhanced t1-weighted mri," *Phys Med Biol* **55**(6), 1719–1734 (2010).
- [8] Heijmink, S. W. T. P. J., Fütterer, J. J., Strum, S. S., Oyen, W. J. G., Frauscher, F., Witjes, J. A., and Barentsz, J. O., "State-of-the-art urologic imaging in the diagnosis of prostate cancer," *Acta Oncol* **50 Suppl 1**, 25–38 (2011).
- [9] Hoeks, C. M. A., Barentsz, J. O., Hambrock, T., Yakar, D., Somford, D. M., Heijmink, S. W. T. P. J., Scheenen, T. W. J., Vos, P. C., Huisman, H., van Oort, I. M., Witjes, J. A., Heerschap, A., and Fütterer, J. J., "Prostate cancer: Multiparametric MR imaging for detection, localization, and staging," *Radiology* **261**(1), 46–66 (2011).
- [10] Amadasun, M. and King, R., "Textural features corresponding to textural properties," *IEEE Trans Syst Man Cybern* **19**(5), 1264–1274 (1989).
- [11] Li, H., Giger, M. L., Olopade, O. I., Margolis, A., Lan, L., and Chinander, M. R., "Computerized texture analysis of mammographic parenchymal patterns of digitized mammograms.," *Acad Radiol* **12**(7), 863–873 (2005).
- [12] Lindeberg, T., "Feature detection with automatic scale selection," *Int J Comput Vis* **30**(2), 79–116 (1998).
- [13] Klein, S., van der Heide, U. A., Lips, I. M., van Vulpen, M., Staring, M., and Pluim, J. P. W., "Automatic segmentation of the prostate in 3D MR images by atlas matching using localized mutual information," *Med Phys* **35**(4), 1407–1417 (2008).
- [14] Huisman, H. J., Engelbrecht, M. R., and Barentsz, J. O., "Accurate estimation of pharmacokinetic contrast-enhanced dynamic MRI parameters of the prostate," *J Magn Reson Imaging* **13**(4), 607–614 (2001).
- [15] Vos, P. C., Hambrock, T., Barentsz, J. O., and Huisman, H. J., "Automated calibration for computerized analysis of prostate lesions using pharmacokinetic magnetic resonance images," in [*Med Image Comput Assist Interv*], *Lect Notes Comput Sci* **12**, 836–843 (2009).
- [16] Moltz, J. H., Bornemann, L., Kuhnigk, J.-M., Dicken, V., Peitgen, E., Meier, S., Bolte, H., Fabel, M., Bauknecht, H.-C., Hittinger, M., Kiessling, A., Pusken, M., and Peitgen, H.-O., "Advanced segmentation techniques for lung nodules, liver metastases, and enlarged lymph nodes in CT scans," *IEEE J Sel Top Signal Process* **3**, 122–134 (2009).
- [17] Chakraborty, D. P., "Maximum likelihood analysis of free-response receiver operating characteristic (froc) data," *Med Phys* **16**(4), 561–568 (1989).
- [18] Pudil, P., Novovicova, J., and Kittler, J., "Floating search methods in feature selection," *Pattern Recognition Letters* **15**(11), 1119–1125 (1994).